Cellular and Molecular Neurobiology (2024) 44:17
https://doi.org/10.1007/s10571-023-01439-0

ORIGINAL RESEARCH

Treadmill Running Regulates Adult Neurogenesis, Spatial and Non-spatial Learning, Parvalbumin Neuron Activity by ErbB4 Signaling

Yandong Yi[1,2] · Yuejin Zhang[2,3] · Yuanlong Song[2,3] · Yisheng Lu[2,3]

Received: 29 June 2023 / Accepted: 6 November 2023

Abstract

Exercise can promote adult neurogenesis and improve symptoms associated with schizophrenia and other mental disorders via parvalbumin (PV)-positive GABAergic interneurons in the dentate gyrus ErbB4 is the receptor of neurotrophic factor neuregulin 1, expressed mostly in PV-positive interneurons. Whether ErbB4 in PV-positive neurons mediates the beneficial effect of exercise and adult neurogenesis on mental disorder needs to be further investigation. Here, we first conducted a four-week study on the effects of AG1478, an ErbB4 inhibitor, on memory and neurogenesis. AG1478 significantly impaired the performance in several memory tasks, including the *T*-maze, Morris water maze, and contextual fear conditioning, down-regulated the expression of total ErbB4 (T-ErbB4) and the ratio of phosphate-ErbB4 (p-ErbB4) to T-ErbB4, and associated with neurogenesis impairment. Interestingly, AG1478 also appeared to decrease intracellular calcium levels in PV neurons, which could be reversed by exercise. These results suggest exercise may regulate adult neurogenesis and PV neuron activity through ErbB4 signaling. Overall, these findings provide further evidence of the importance of exercise for neurogenesis and suggest that targeting ErbB4 may be a promising strategy for improving memory and other cognitive functions in individuals with mental disorders.

Yandong Yi and Yuejin Zhang have contributed equally to this work.

✉ Yisheng Lu
Luys@hust.edu.cn

Yandong Yi
yandong_y@163.com

Yuejin Zhang
yuejingzhang1@outlook.com

Yuanlong Song
songyuanlong@hotmail.com

[1] Department of Pharmacy, Traditional Chinese and Western Medicine Hospital of Wuhan, Tongji Medical College, Huazhong University of Science and Technology, Wuhan 430030, China

[2] Department of Physiology, School of Basic Medicine, Huazhong University of Science and Technology, Wuhan 430030, China

[3] Institute of Brain Research, Collaborative Innovation Center for Brain Science, Huazhong University of Science and Technology, Wuhan 430030, China

Published online: 29 January 2024

Graphical Abstract

Treadmill running and ErbB4 signaling: AG1478 downregulated the expression of T-ErbB4 and the ratio of p-ErbB4 to T-ErbB4, while treadmill running enhanced neurogenesis, increased spatial learning and memory, non-spatial working, and reference memory and promoted the intracellular Ca^{2+} levels in PV neurons.

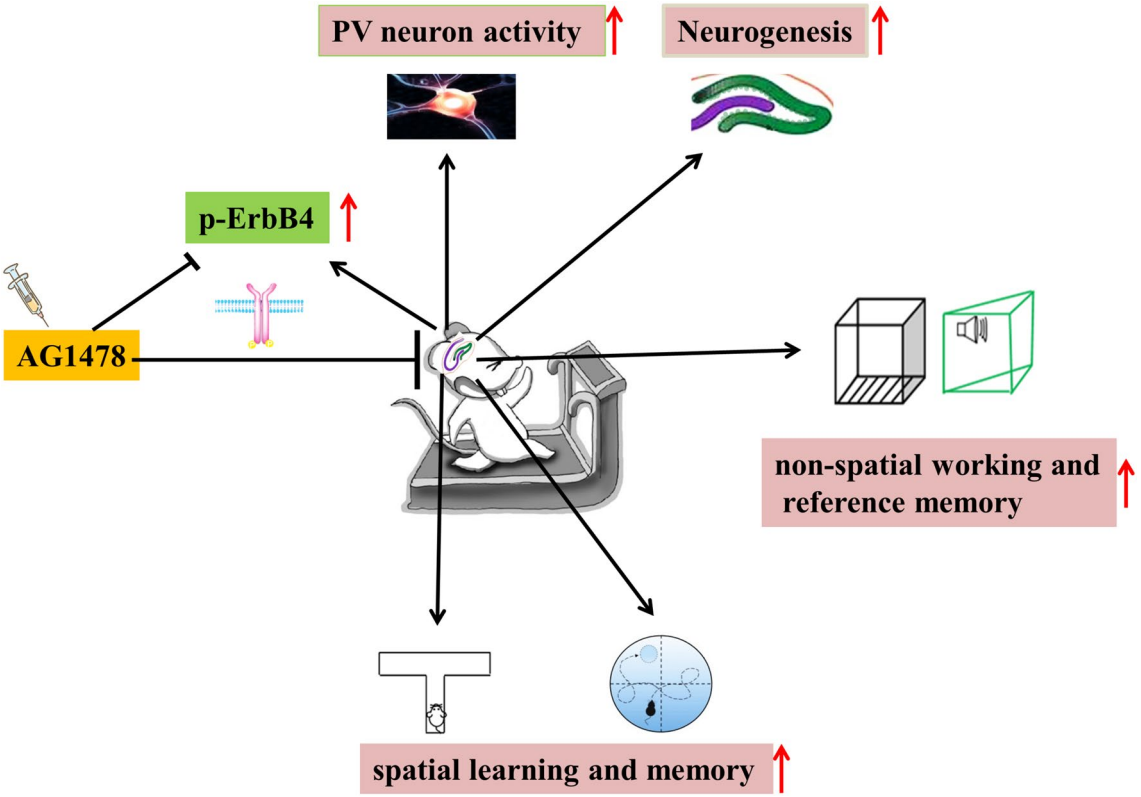

Keywords Treadmill running · Neurogenesis · ErbB4 · Fear conditioning · Spatial memory · AG1478

Introduction

The subgranular zone of the dentate gyrus (DG) in the brain is responsible for adult neurogenesis, which plays an important role in cognitive functions (Christian et al. 2014). Impairment of neurogenesis in the DG is associated with neuropsychiatric disorders, including bipolar disorder and schizophrenia. (Mao et al. 2009; Mertens et al. 2015). Physical exercise and enriched environments can improve cognitive functions through promotion of hippocampal neurogenesis (Kempermann et al. 1997; Pajonk et al. 2010). Parvalbumin (PV)-positive GABAergic interneurons in the DG are critical for the beneficial effects of exercise on adult neurogenesis to alleviate schizophrenia-related phenotypes in mouse models (Yi et al. 2020). However, the cellular and molecular mechanisms are still not yet clear. ErbB4, a receptor of the neurotropic factor neuregulin 1 (NRG1), is a susceptibility gene for schizophrenia and bipolar disorder, and critical for the activity-dependent release of GABA in the hippocampus (Deng et al. 2013; Mei and Xiong 2008). ErbB4 is mostly expressed in PV-positive interneurons. Knockout ErbB4 in PV interneurons cause cognitive impairments, and inhibit neurogenesis in the DG (Zhang et al. 2018). Our previous study also observed an increase in ErbB4 expression in the hippocampus induced by exercise, however, whether NRG1/ErbB signaling affects PV interneuron function to mediate exercise effects on adult neurogenesis is still unknown.

To investigate the effects of ErbB4 on neurogenesis and behavioral phenotypes for running, we pharmacologically inhibit ErbB4 by AG1478, and observed its effects on anxiety-like behavior and spatial reference memory impairments, as well as adult neurogenesis and intracellular Ca^{2+} levels in PV neurons. Results showed that AG1478 treatment increased spatial learning and memory, non-spatial working, and reference memory impairments, but

not anxiety-like behavior, decreased adult neurogenesis, and intracellular Ca^{2+} levels in PV neurons.

Interestingly, we also found that treadmill running could have protective effects against the adverse effects of ErbB4 inhibition. These results suggest that of ErbB4 signaling may be a key mechanism for PV-positive interneuron mediating the positive effects of exercise on adult hippocampus neurogenesis.

Materials and Methods

Animal

C57BL/6 J male mice (7 weeks old) were purchased from the Experimental Animals Center of Tongji Medical College, Huazhong University of Science and Technology. All mice experiments in this research were carried out following the recommendations of, and were approved by the Animal Welfare Committee of Huazhong University of Science and Technology.

The mouse strains used included wild-type C57BL/6 J, PV-Cre mice. C57BL/6 male mice (7 weeksold) were purchased from the Experimental Animals Center of Tongji Medical College, Huazhong University of Science and Technology. PV-Cre mice were described previously (Wen et al. 2010), PV-Cre mouse line (Stock No. 017320, Jackson Laboratory) used was kindly provided by Dr. Lin Mei (Case Western Reserve University). Tail genomic DNA was used for genotyping by PCR. A 300-bp fragment was detected for the PV-Cre allele.

Mice aged between 7 and 14 weeks were used for all experiments. Animals were housed in less than 5 mice per cage at 22–24 °C with 40–70% humidity, on a 12 h/12 h light/dark cycle schedule, with water and food available ad libitum. Mice were all backcrossed with C57BL/6 J mice for over 10 generations.

Experimental Design

Protocols for animal experiments were approved by the Animal Experimental Ethics Committee of the Huazhong University of Science and Technology (Approval Code: 82071508) on September 27, 2020. Each experiment and the statistical calculations described below were carried out in a randomized order by the experimenter blinded to the group. A schematic experimental design is shown in Fig. 1. AG1478 (HY-13524, MCE) was solubilized in DMSO and diluted to a concentration of 10 mg/kg mouse weight in sterile saline. AG1478 or saline (1% DMSO in normal saline), at a dose of 50 mg/kg body weight, was chronically administered intraperitoneally (i.p.) for 2 h before running every other day for four weeks. The timing and dose of AG1478 administration was based on a previous study (Weglicki et al. 2012).

The procedures have been described previously (Yi et al. 2020). The mice in running groups underwent adaptive run-training sessions in individual lanes of a treadmill (FT-200, Taimeng, China) (5 m/min for 45 min) for 5 days, and running sessions (5 m/min for 10 min, 8 m/min for 30 min, 5 m/min for 10 min) for the next 4 weeks to prevent stress-induced inhibition of hippocampal neurogenesis (Leem et al. 2018). Mice in the static groups were placed on the stationary treadmill for the same duration, and they often did not move or move by themselves. The running time is fixed in the morning.

BrdU Injections

5′-bromo-2′-deoxyuridine (BrdU; Sigma) in saline was administered i.p. 1 h before running every 4 hours (100 mg/kg), twice 1 day, for 6 days. Animals were sacrificed five weeks after the last BrdU injection.

Behavioral Analysis

All behavioral tests were performed during light periods, and all mice were handled for at least 5 min twice a day for 3 days before the behavioral test (Albarran-Zeckler et al. 2012). Behavioral analysis was performed on 12-week-old mice by investigators unaware of their genotype and groups.

Animals were tested in sequential order of least disruptive (absence of noxious stimulation: open field and *T*-maze) to most disruptive (e.g., MWM, fear conditioning test, and contextual fear discrimination learning, which involved physical stimuli, such as loud noise, foot shock, or cool water).

Open Field Test (OFT)

To provide measures of locomotor activity and general anxiety-like behavior, locomotor activity was recorded in the open field, made of a rectangular chamber (45 × 45 × 45 cm). The floor illumination level is set to 200 lux by LED lights on both sides of the wall. The mouse was gently placed on the center square and allowed to freely explore the arena for 5 min. The total distance traveled during a session, the time spent moving, and the total duration spent in the center were measured by an automated video tracking system (TMV-100S, TaiMeng, China) above the open field. After each trial, the apparatus was swept out with 75% alcohol to avoid the presence of olfactory cues. General activity and anxiety

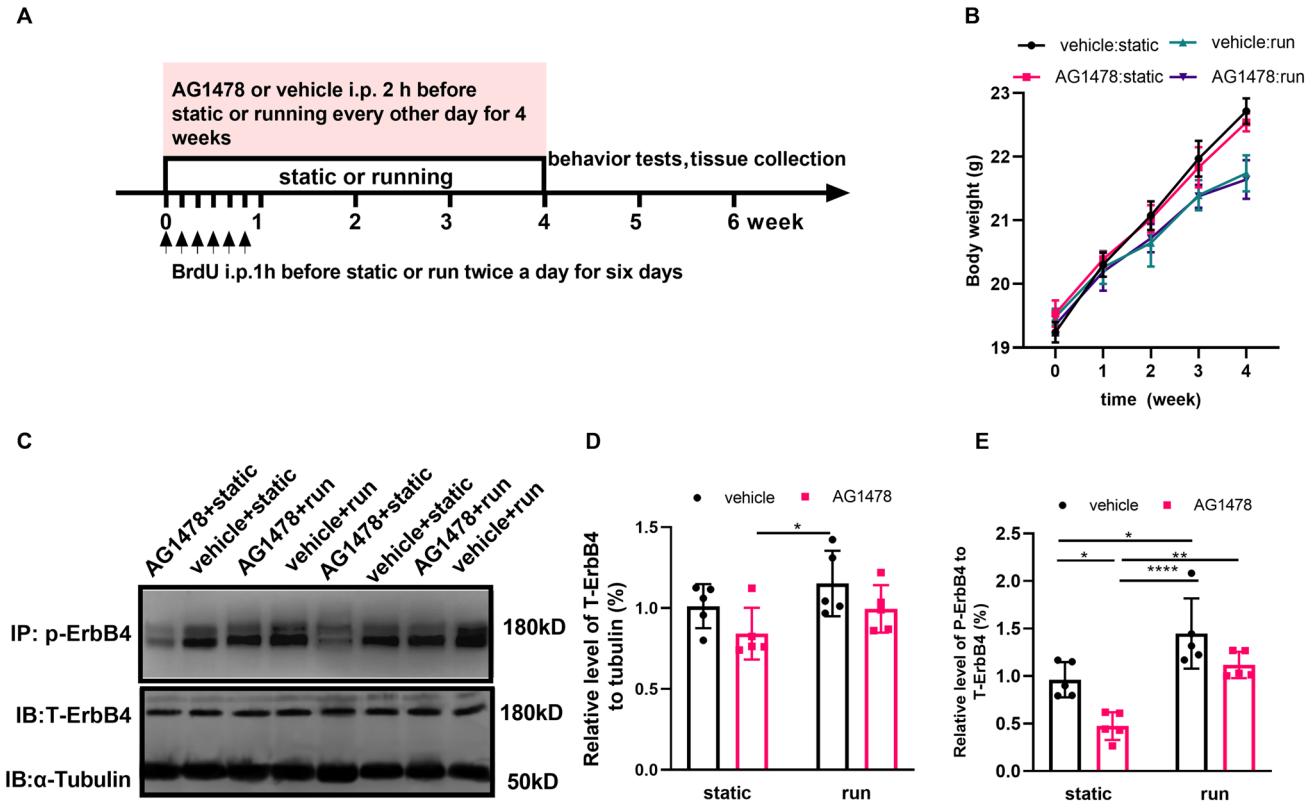

Fig. 1 AG1478 neutralized treadmill running effect on ErbB4 phosphorylation in the hippocampus. **A** Schematic experimental design. **B** The body weight of both the vehicle:run group and AG1478: run group weighs less than the relevant control group (vehicle: static group and AG1478: static group), while AG1478 does not affect it. Data are expressed as mean ± SEM, Three way ANOVA: F (4, 180) = 862.7, $p < 0.0001$; Tukey's multiple comparisons test: in the 2nd week: vehilce: static vs. vehicle:run: $p = 0.0096$, AG1478: static vs. vehicle: run: $p = 0.0477$, in the 3rd week: vehilce: static vs. vehicle: run: $p < 0.0001$, AG1478: static vs. AG1478: run: $p = 0.0038$, AG1478: static vs. vehicle: run: $p = 0.0070$, in the 4th week: AG1478: static vs. AG1478: run: $p < 0.0001$, AG1478: static vs. vehicle: run: $p < 0.0001$, vehicle: static vs. AG1478: run: $p < 0.0001$, vehicle: static vs. vehicle: run: $p < 0.0001$, *$p < 0.05$, ****$p < 0.0001$. $n = 8$. **C** Representative western blots of total ErbB4 and phosphate-ErbB4 in the hippocampus. a-Tubulin was used for normalization. $n = 5$. **D** Quantitative analysis of the expression of total ErbB4 in the hippocampus. Two way ANOVA: F (1, 16) = 0.008286, $P = 0.9286$, Tukey's multiple comparisons test: AG1478: static vs. vehicle: run: $p = 0.0385$. **E** Quantitative analysis of the relative phosphate-ErbB4 level to total ErbB4 in the hippocampus. $n = 5$, Two way ANOVA: F (1,16) = 0.5757, $p = 0.4590$, Tukey's multiple comparisons test: vehicle: static vs. AG1478:static: $p = 0.0242$, vehicle:static vs. vehicle: run: $p = 0.0245$, vehicle:run vs. AG1478: static: $p < 0.0001$, AG1478:static vs. AG1478:run: $p = 0.0026$

were assessed by calculating the total distance traveled, total movement time, and time spent in the center of the field, respectively.

Forced-Choice Spontaneous Alternation in *T*-Maze *Test*

A forced-choice paradigm was employed to encourage a higher level of alternation (Hughes 2004). The apparatus was an enclosed maze with 3 arms, a start arm (38 × 7 cm), a central choice area (7 × 7 cm), and two symmetrically choice arms (30 × 7 cm). In brief, each trial consisted of a 5-min acquisition phase, an inter-trial interval (ITI; 2 min), and a final 5-min test phase. ITIs of 2 min were included to assess the persistence of short-term spatial memory (Lalonde et al. 2003). During the acquisition phase, the mouse was placed in the starting arm facing the wall and allowed to explore the apparatus. As soon as the animal entered (with all four paws) one of the two choice arms, the compartment door was closed for 30 s. Then, the mouse was gently removed from the maze to the home cage for the ITI. At the test, the block was removed, and the mouse was placed back in the starting arm for a second-choice trial. The novel arm in the second trial was the right choice, the arena was thoroughly cleaned using 70% ethanol to remove any scent cues, that could identify the novel arm. The test was conducted in the room where the animals were housed and consisted of 10 trials.

$$\text{Correct percentage (\%)} = \frac{\text{total novel arm in the second trials}}{\text{total trials}} \times 100\%$$

Contextual and Cued Fear Conditioning Test

The contextual and cued fear conditioning test is the behavioral paradigm used to evaluate associative fear learning, hippocampus-dependent, and hippocampus-independent memory function memory in rodents (Shoji et al. 2014). Briefly, the mouse was placed in the conditioning chamber using the Freeze Monitor system (San Diego Instruments, San Diego, CA, USA) for 3 min as an accommodation period and then a tone-foot-shock pairing (tone, 30 s, 65 dB, 1 kHz; foot shock, 2 s, 0.75 mA) was delivered. The mouse was allowed to explore the chamber for another 30 s after the shock to study postshock freezing.

The contextual fear conditioning test was assessed 24 h after training by placing the mice back in the same test chamber for 3 min to assess short-term memory. The floor illumination level is set to 100 lux by LED lights. The cued fear conditioning test was assessed 2 h after the contextual fear conditioning test in a novel acrylic triangular chamber with a flat, white floor, covered with a transparent lid chamber (context C) changed smell (A drop of lemon juice on one wall) and tone of the training for 3 min. The floor illumination level is set to 30 lux by LED lights.

Freezing behavior, defined as the absence of all visible movement of the body except the movement necessitated by respiration, was scored by a observing software. At the end of each test, the chamber was cleaned with 75% alcohol to avoid the presence of olfactory cues.

Morris Water Maze

To assess hippocampal-dependent spatial learning and memory, mice were tested in the Morris water maze (MWM,XR-XM101; Shanghai Softmaze Information Technology Co., Ltd., Shanghai, China) (130 cm diameter, 45 cm high) containing opaque water (24–26 °C) and a circular platform (10 cm diameter, approximately 1 cm below the water surface) located in the center of the target quadrant. The MWM was virtually divided into four equal imaginary quadrants by the AnyMaze software. The test was executed as previously described (Montag-Sallaz and Montag 2003). Briefly, the test consisted of a 4-day hidden platform training test and a one-day single probe test. In the training test, the mouse was allowed to face the pool wall in a random starting place to find the hidden platform. The mouse was allowed 120 s to find the platform they sat for 20 s. If the mouse did not find the platform within 120 s, it was gently guided there and allowed to stay on it for 30 s. Twenty-four hours after the last training session, the platform was removed from the pool, the mouse was placed in the opposite quadrant, and a 60-s probe trial was performed. The escape latency, the percentage of time spent on the target, and the number of platform crossings were recorded.

Contextual Fear Discrimination Learning

Pattern separation is a fundamental computational function of DG (Faghihi and Moustafa 2015; McNaughton et al. 1986), which depends on normal adult neurogenesis. This paradigm tests the animal's ability to distinguish between similar contexts (Sahay et al. 2011). The shock-associated training context A (with foot shock) and the similar context B (without foot shock) shared many features, including an exposed stainless-steel grid floor and roof. Four black and white inserts were applied to cover the walls, and a plexiglass floorboard was above the stainless-steel grid floor in context B. A non-alcoholic antiseptic solution was used to clean the grids between trials. In pilot experiments, mice were exposed to context A, where they received a single 2 s 0.75 mA foot shock, 185 s following placement in the soundproof chamber (29 × 29 × 24 cm; Coulbourn instruments, Allentown, PA, USA, model H10-11 M-7C-SF) and the floor's illumination level is set to 100 lux by the LED lights. In discrimination learning, mice were exposed to the training context A. One hour later, mice were placed in a similar context C, and left for 180 s without foot shocks. When no mouse movement is detected for more than 2 s, its behavior is counted as "freezing."

Freezing behavior during the test is tracked and measured as an index of fear memory using video tracking software daily. Context discrimination ratio was calculated as follows: a score of 0 indicated a complete lack of discrimination, i.e., freezing levels were the same in similar and training contexts (Freezing similar context = Freezing training context).

$$\text{Discrimination ratio} = \frac{\text{Freezing training context A} - \text{Freezing similar context B}}{\text{Freezing training context A} + \text{Freezing similar context B}}$$

In Vitro and In Vivo Calcium Imaging

To assess the effect of AG1478 on intracellular Ca^{2+} levels in PV neurons, calcium signals from cells were observed in brain slices. First, the brain slice was quickly removed and placed in 4 °C artificial cerebrospinal fluid (ACSF) composed of (in mM) choline chloride 110, KCl 2.5, NaH_2PO_4 1.25, $NaHCO_3$ 26.0, $CaCl_2$ 0.5, $MgCl_2$ 7, d-glucose 10, Na-ascorbate 11.6, Na-pyruvate 3.1, and atropine sulfate 0.01. The coronal slices (300 µm) were cut using a Leica VT1000S vibratome and then incubated in standard ACSF containing (in mM) NaCl 126, KCl 3, NaH_2PO_4 1.25, $NaHCO_3$ 26.0, $CaCl_2$ 2, $MgSO_4$ 2, d-glucose 11 saturated with 95% O_2 and 5% CO_2. Next, hippocampus slices were kept at 32 °C for approximately 30 min before recording. The Ca^{2+} signals were visualized by an inverted fluorescent microscope (Olympus, USA) with

a water-immersion objective lens (40X, LUMPlanFL, 0.80 numerical aperture; OLYMPUS). Brain slices from one animal were divided into two groups. One group was incubated for 30 min at 32 °C in ACSF as the control group, whereas another in 10 μmol/L AG1478 as the experiment group. Upon excitation at 488 nm, calcium-complexed GCaMP6 was collected at ten frames per second using the Image-pro plus 7.0 software. The Ca^{2+} levels in slices were calculated as following using calcium imaging in vitro assay.

To further assess the effect of AG1478 on intracellular Ca^{2+} levels in PV neurons of the running mice, calcium signals from cells in awake animals with head-fixed animals were observed by in vivo calcium imaging. Firstly, 300 nL of AAV-EF1α-DIO-GCaMP6m-WPRE-hGH-pA viruses (BrainVTA, catalog# PT-0283) were injected into the DG of PV-Cre mice using a stereotaxic instrument. The stereotactic technology procedures have been described previously (Yi et al. 2020). Adult PV-Cre mice were anesthetized with chloral hydrate (400 mg/kg, i.p.) and head-fixed in a stereotaxic device (RWD Life Science; 68,025). Viruses were unilaterally injected (0.3 mL per side, 0.05 nL/min) with a glass pipette (Cetin et al. 2006) (tip size, ~ 20 mm) at the following coordinates relative to bregma: anteroposterior, − 1.94 mm; dorsoventral, − 2.14 mm; and mediolateral, ± 1.5 mm. After injection, the glass pipette was left in place for 15 min before slowly removing it. The titers of AAV-EF1α-DIO-GCaMP6m-WPRE-hGH-pA (BrainVTA, catalog #: PT-0283) were 2×10^{12} genome copies per mL. Secondly, 4 weeks after virus injection, the gradient-index (GRIN) lens (0.5 mm in diameter and 5.901 mm in length, Gofoton, USA, GRIN Tech) was firmly mounted to a stereotaxic holder. The GRIN lens were inserted into the DG (either the left or the right side) and positioned at 0.10 mm to 0.20 mm above the highest viral injection site. Next, dental cement (New Century Dental Materials Co. Ltd., Shanghai, China) was applied to secure the GRIN lens. During recording, the distance from the microscope to the GRIN lens was adjusted by a micro-manipulator until the field of view was in focus. The gain was set at 16, and the LED (470 nm) power was maintained at 100%. Images were collected at 30 frames per second using the MiniScope V2.0 software.

In vivo Ca^{2+} imaging experiments, we divided the mice into two groups. Both groups received a dose of vehicle, and the Ca^{2+} signals in the static state were recorded 30 min later. Subsequently, one group continued to receive vehicle, while the other group was administered AG1478. Ca^{2+} signals were recorded once more after another 30 min. Finally, following a period of running exercise, we recorded the Ca^{2+} signals again. All comparisons were based on the Ca^{2+} signal intensity recorded during the static state.

Images were processed using MATLAB R2020b (Mathworks, Natick, MA) with customized code (https://github.com/thinkertech333/analysisforminiscope, Thinkertech, Nanjing, China), and Cellsort 4.0 software. After motion correction (set at 10) and denoising (set at 100), the region of interest was manually selected according to the fluorescence intensity. The Ca^{2+} signals in the first 5 s were considered baseline, and the average Ca^{2+} signal in this period was used as a reference (F0) to normalize the fluorescence signal (DF/F). The formula is as follows:

$$\Delta F/F = \frac{F_{signal} - F0}{F0}$$

F_{signal} is the real-time Ca^{2+} signal intensity of the cells of interest, F0 is the average Ca^{2+} signal intensity in the baseline period.

Immunofluorescence

Mice were anesthetized with chloral hydrate and perfused transcardially with 4% paraformaldehyde (PFA) in phosphate-buffered saline (PBS, pH7.4), and tissues were fixed overnight in 4% PFA at 4 °C. After cryoprotected in 30% sucrose, brain tissues were frozen in OCT and cut into 40 μm by a cryostat (Thermo Scientific, HM550).

The free-floating sections were rinsed three times in PBS, blocked in PBS with 0.3% Triton and 10% goat serum, and 0.1% Triton-X 100 (PBST) for 60 min at room temperature. Sections were then incubated with primary antibodies in PBST at 4 °C overnight. After washing with PBS 3 times, samples were incubated with second antibodies in PBST for 1 h at room temperature. Samples were mounted with mounting medium, antifading (with DAPI) (S2110, Beijing Solarbio Science & Technology), and images were taken with a Zeiss Axioplan light microscope. Label quantification of labeling was determined by counting all fluorescent cells in 3–5 sections per animal. Adobe Photoshop CS6 (PS) software was used to calculate the areas of the DG. Next, we used the counting tool to count the number of cells in the target area. The density of positive cells was calculated by the number of positive cells divided by the area of the DG.

For BrdU staining, sections were incubated with 2 N HCl for 30 min at 37 °C to denature the DNA, followed by neutralization with 0.1 M borate buffer (pH 8.5) for 10 min at room temperature. After neutralization, sections were rinsed with PBS several times before incubation with primary antibodies.

Immunocytochemistry used following antibodies: rabbit anti-KI67 (1:500, Abcam, Cambridge, UK, catalog #: ab15580, PMID: 34420159), rat anti-BrdU (1:300, FITC conjugated, Abcam, Cambridge, UK, catalog #:ab74545, PMID: 32117963), mouse anti-NeuN (1:500, Abcam, Cambridge, UK, catalog #: ab104224, PMID: 32117963), rabbit anti-PV (1:100, Abclonal, Shanghai, CN, catalog #: A2791,PMID: 32117963), donkey anti-rabbit IgG

conjugated with Alexa Fluor 594 (1:200, Jackson ImmunoResearch, USA, catalog #: R37119, PMID: 32117963), goat anti-rabbit IgG conjugated with Alexa Fluor 488 (1: 250, Proteintech, CN, catalog #: SA00006-2, PMID: 30208760), goat anti-mouse 488(1:250, Proteintech, CN, catalog #: SA00013-1, PMID: 31849642).

Western Blot

One day after behavioral tests, the mice were anesthetized with 5% chloral hydrate (8 ml/kg), and tissues were rapidly collected. The tissue homogenates were prepared on ice in RIPA buffer containing 50 mM Tris-HCl (pH 7.4), 150 mM NaCl, 5% sodium deoxycholate, 1% NP40, 1 mM PMSF, and 1 μg/ml protease inhibitor cocktail. For immunoblotting p-ErbB4, homogenates were subjected to immunoprecipitation with ErbB4 antibody and protein-A (Roche) at 4 °C overnight. Homogenates or bound proteins were resolved on SDS/PAGE and transferred to PVDF membranes, which were incubated in Tris–Phosphate buffer (TBS) containing 0.1% Tween-20 and 5% milk (TBST) for 1 h at room temperature before the addition of primary antibodies for incubation overnight at 4 °C. After washing, the membranes were incubated with HRP-conjugated secondary antibodies (1: 30000, Biosharp, catalog #: BL003A, PMID: 32117963) in TBS for 1 h at room temperature. Primary antibodies used and blotting conditions were: rabbit anti-phosphate-ErbB4 (1:1000, Abcam, Cambridge, UK, catalog #: Ab76132, PMID: 31043588), ErbB4 (1:1000, catalog #: ab19391, Cambridge, UK), rabbit polyclonal anti-a-Tubulin (AC003, 1:500, Abclonal, Abclonal, Shanghai, CN, PMID: 32117963). These bands were visualized using enhanced chemiluminescence (Biorad, UK, catalog #: 1705060), scanned by MicroChemi 4.2 (DNR Bio-imaging Systems, ISRAEL), and quantified with Image J software (National Institutes of Health, Bethesda, MD, USA). Protein levels were quantified by measuring the density of each band using Image J software and then normalized to the α-Tubulin level.

Statistical Analysis

All statistical analyses were performed by GraphPad Prism 8.0 Software (GraphPad Software, San Diego, CA) and detailed in the corresponding figure legends. The quantitative data were expressed as Mean ± SEM. Group comparisons were made using two-way ANOVA followed by Tukey's post hoc tests for multiple comparisons. A mixed 3-way ANOVA was applied in case of repeated measurements (for instance, for the body weight in Fig. 1B, the open field data in Fig. 3B, and pattern separation in Fig. 5H) with "running" and "treatment" as between groups factors and "time bins" as within groups factor. *$p < 0.05$, **$p < 0.01$, ***$p < 0.001$, ****$p < 0.0001$. Comparisons with no asterisk or 'NS' had $p > 0.05$ and were considered not significant.

Results

AG1478 Neutralized Treadmill Running Effect on ErbB4 Phosphorylation in the Hippocampus

AG1478, an ErbB signaling inhibitor, has been shown to block exercise-induced NRG1/ErbB signaling transduction in the heart (Cai et al. 2016). To investigate the effect of treadmill running on ErbB4 signaling activation in the brain, AG1478 was administered 2 h before each treadmill session. The animals were randomly assigned into four groups according to treatment: (1). AG1478: static: the group subjected to daily AG1478 injection and static treadmill, (2). vehicle: static: the group subjected to saline injection and static treadmill, (3). AG1478: run: the group subjected to daily AG1478 injection and running treadmill, (4). vehicle: run: the group subjected to saline injection and running treadmill (Fig. 1A). Consistent with the previous study (So et al. 2017), all groups gained weight, but the two running groups weight gain was less than the two static groups.. However, AG1478 did not affect body weight within 4 weeks (Fig. 1B). One day after behavioral tests, the mice were anesthetized, and tissues were collected rapidly. The immunoprecipitation assay was conducted to further detect ErbB4 phosphorylation. No change in total ErbB4 protein levels was observed in AG1478: static and vehicle: static mice (Fig. 1C, D), However, vehicle: run mice exhibited significant upregulation of ErbB4 phosphorylation (Y1258) and total ErbB4 expression in the hippocampus compared to the AG1478: static group. In contrast, significant reductions in relative pErbB4 levels to total ErbB4 were observed in AG1478: static mice compared to the vehicle: static group. These decreased levels in the hippocampus of AG1478: static mice were attenuated by running (Fig. 1C, E).

AG1478 Neutralized Treadmill Running Effect on NSCs Survival and Proliferation in the DG

To investigate cell survival, BrdU was injected during the first week of treadmill running to label proliferating progenitor cells. NeuN was used as a neuron marker of postmitotic steps to assess their maturation. Ki67, a marker of intrinsic proliferating cells, was observed at the end of training. As shown in Fig. 2A, the number of Ki67 cells decreased in the AG1478: static compared to the vehicle:static. In line with numerous reports (van Praag et al. 1999), treadmill running enhanced the proliferation

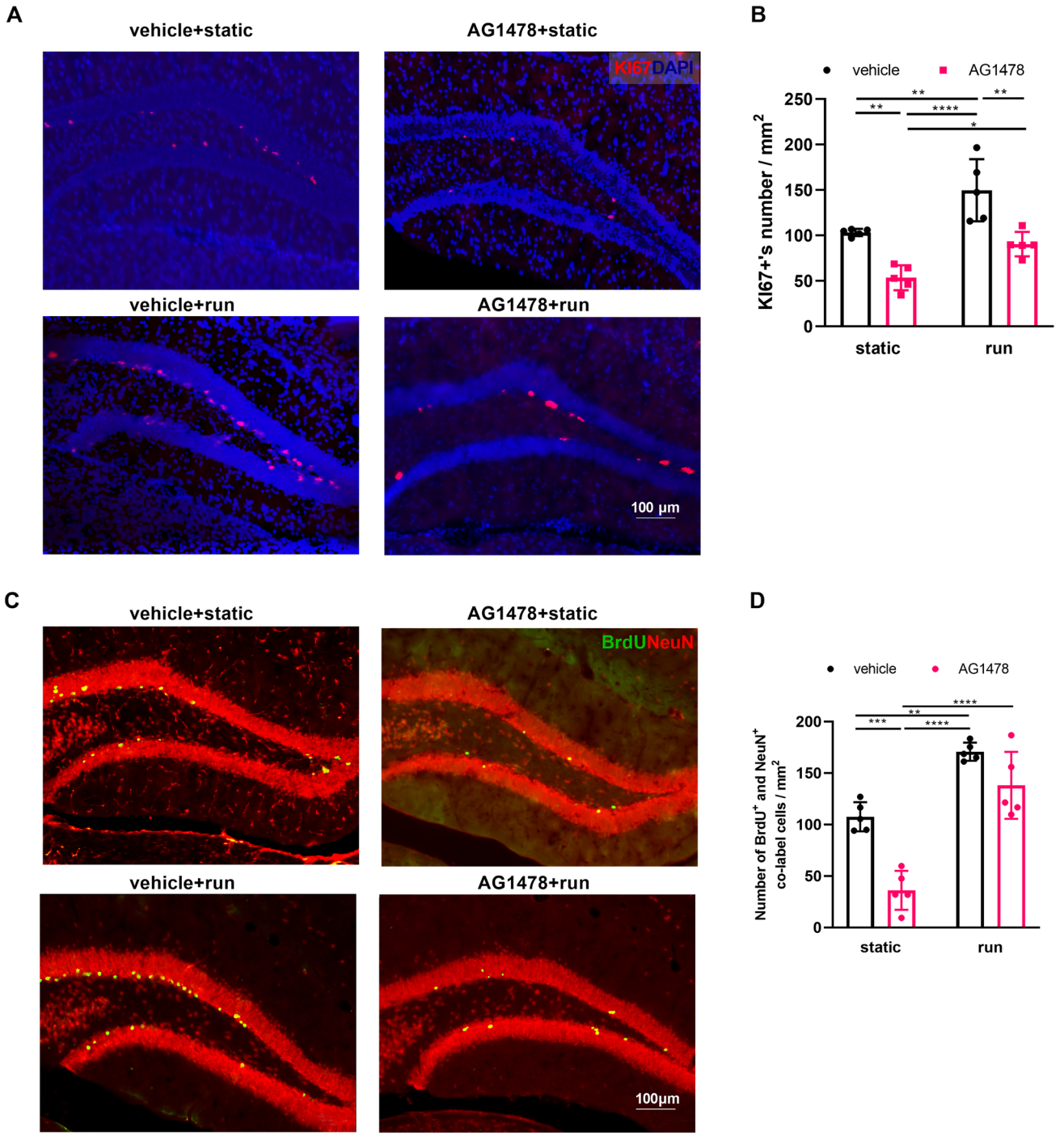

Fig. 2 AG1478 neutralized treadmill running effect on NSCs survival and proliferation in the DG. **A** Representative images of Ki67$^+$ cells and DAPI in the DG. Scale bar, 100 μm. **B** Quantification of Ki67$^+$ cells reveals a significant decrease in their total number in the AG1478: static mice when compared to vehicle: static mice, which are increased by running. Two way ANOVA: F (1, 16) = 0.2847, $p = 0.6009$, Tukey's multiple comparisons test: vehicle: static AG1478: static vs. AG1478: static $p = 0.0051$, vehicle: static vs. vehicle: run: $p = 0.0090$, AG1478: static vehicle: run vs. AG1478: static: $p < 0.0001$, AG1478: static vs. AG1478: run: $p = 0.0407$, AG1478: run vs. vehicle: run: $p = 0.0011$, $^{**}p < 0.01$, $^{****}p < 0.0001$. $n = 5$ mice in each group, 5 section per mice. **C** Representative images of BrdU$^+$ cells and their colocalization with NeuN in the DG. Scale bar, 100 μm. **D** Quantification of BrdU $^+$NeuN$^+$ cells reveals a significant decrease in the AG1478: static mice when compared to vehicle: static mice, which are increased by running. Two way ANOVA: F (1, 16) = 4.446, $p = 0.0511$, Tukey's multiple comparisons test: vehicle:static vs. AG1478: static: $p = 0.0003$, vehicle: static vs. vehicle: run: $p = 0.001$, AG1478: static vs. AG1478: run: $p < 0.0001$, AG1478: static vs. vehicle: run: $p < 0.0001$, $^{**}p < 0.01$, $^{****}p < 0.0001$. $n = 5$ mice in each group, 3 section per mice

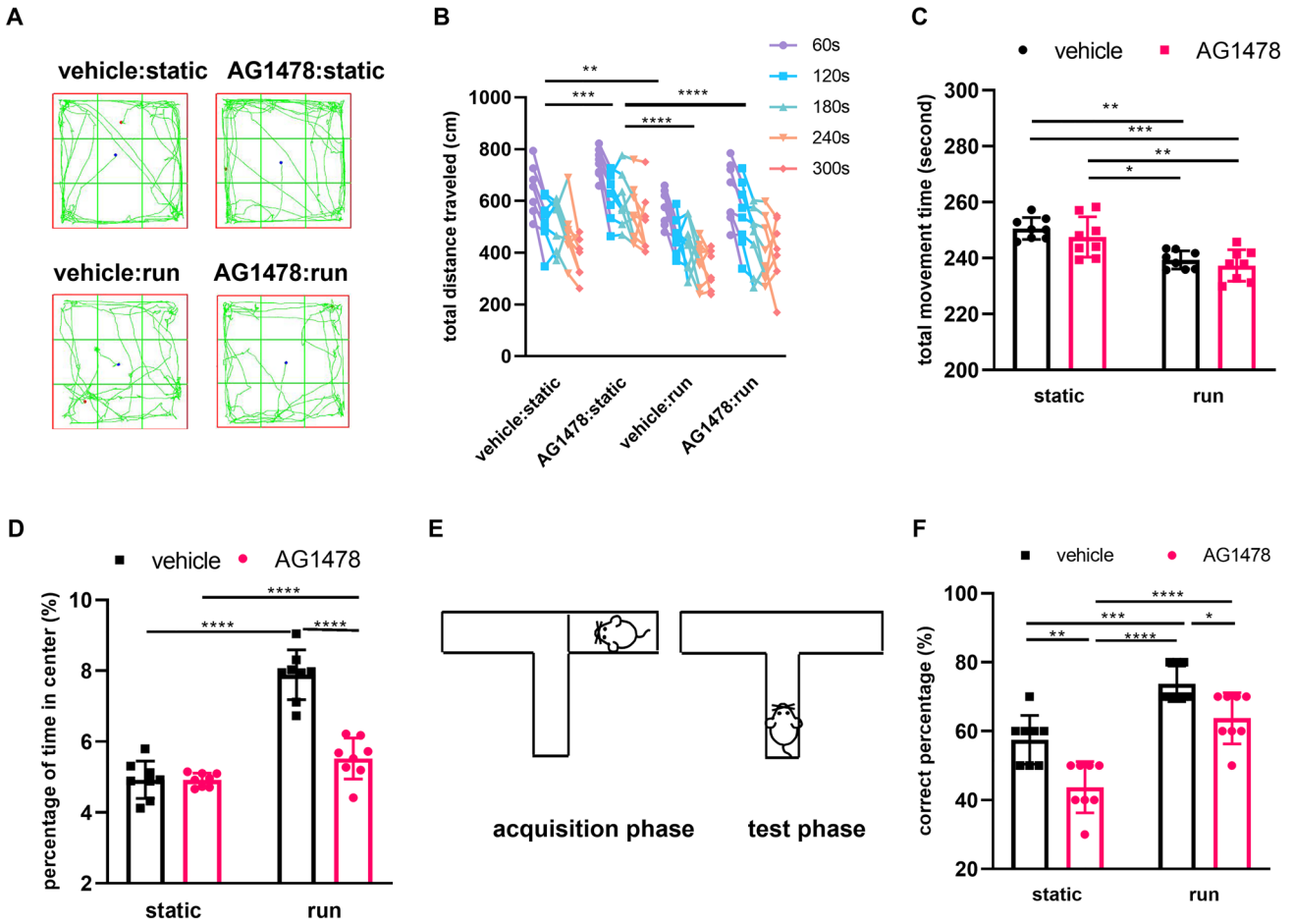

Fig. 3 Treadmill running beneficial effect on hyperactivity, but not anxiety neutralized by AG1478. **A** Representative traces of mice movement during the open field test. Test duration: 5 min. **B** The total movement distance traveled. Three way ANOVA: F (12, 140) = 0.2786, $p = 0.9918$, Tukey's multiple comparisons test: vehicle: static vs. AG1478: static: $p = 0.0001$, vehicle: static vs. vehicle: run: $p = 0.0058$, AG1478: static vs. vehicle: run: $p < 0.0201$, AG1478: static vs. AG1478: run: $p < 0.0001$. *$p < 0.05$, ***$p < 0.001$, ****$p < 0.0001$. $n = 8$. **C** The total movement time travelled. Three way ANOVA: F (1, 28) = 0.08744, $p = 0.7696$, Tukey's multiple comparisons test: vehicle: static vs. vehicle: run: $p = 0.0010$, vehicle: static vs. AG1478: run: $p = 0.0001$, AG1478: static vs. vehicle: run: $p = 0.0201$, AG1478: static vs. AG1478: run: $p = 0.0031$. *$p < 0.05$, ***$p < 0.001$, ****$p < 0.0001$. $n = 8$. **D** The percentage of time spent in the center of the field. n = 8. Two way ANOVA: F (1, 28) = 38.61, $p < 0.0001$, Tukey's multiple comparisons test: vehicle: static vs. vehicle: run: $p < 0.0001$, AG1478: static vs. vehicle: run: $p < 0.0001$, AG1478: static vs. AG1478: run: $p < 0.0001$. ****$p < 0.0001$. $n = 8$. **E** Schematic illustration of the *T*-maze test. **F** The correct percentage of the right arm in the T-maze test. Two way ANOVA: F (1, 28) = 0.6000, $p = 0.4451$, Tukey's multiple comparisons test: vehicle: static vs. vehicle: run: $p = 0.0022$, vehicle: static vs. vehicle: run: $p = 0.0003$, AG1478: static vs. vehicle: run, $p < 0.0001$, AG1478: static vs. AG1478: run: $p < 0.0001$, vehicle: run vs. AG1478: run: $p = 0.0326$. ***$p < 0.001$, ****$p < 0.0001$. $n = 8$

of NSCs in the DG of the vehicle:run group. The population of Ki67-positive cells was also increased in the vehicle:run compared to AG1478: run (Fig. 2B). Upon analyzing the late BrdU and postmitotic (NeuN) neuronal cells, the AG1478: run group exhibited an elevated population of NeuN/BrdU-positive cells in comparison to AG1478: vehicle, however, no significant change was observed between the AG1478: run group and vehicle: run group (Fig. 2C, D). These results indicate that the effect of exercise on adult neurogenesis in the DG might depend on Erb signaling.

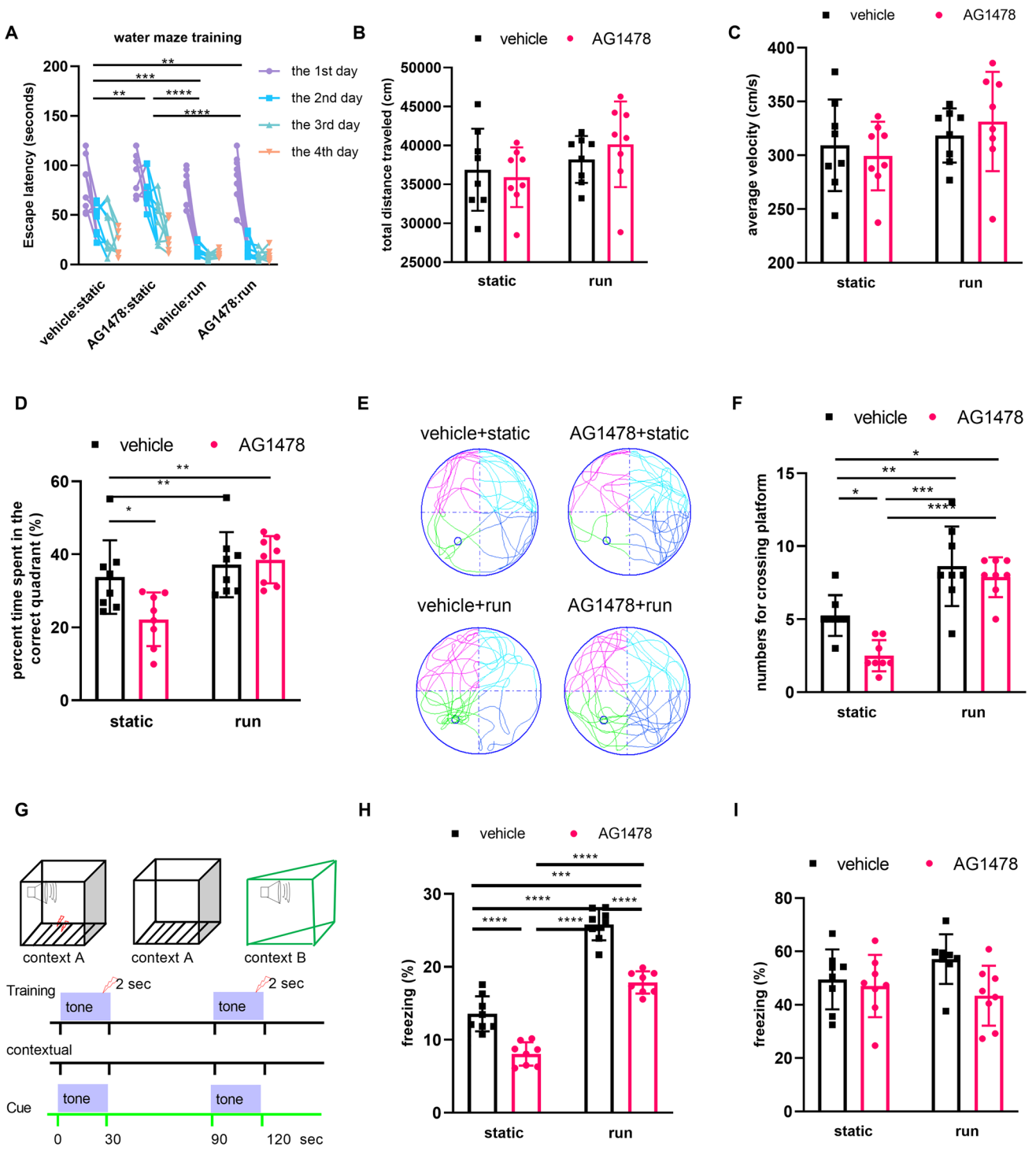

Treadmill Running Beneficial Effect on Hyperactivity, but not Anxiety Neutralized by AG1478

To investigate the effect of AG1478 treatment on locomotor activity and anxiety-like behaviors, we used the open field test (Fig. 3A). AG1478-treated static animals exhibited a robust increase in total distance traveled, while AG1478-treated running mice showed significant decreases in total distance traveled. Importantly, there was no difference between AG1478-treated running mice and vehicle-treated static mice (Fig. 3B), suggesting that running effectively ameliorates hyperactivity through ErbB4 signaling.

Furthermore, when looking at the total movement time and time in the center of the arena, the vehicle-treated running mice exhibited remarkable less anxiety-like behavior

◂**Fig. 4** AG1478 partially compromised movement-dependent effect on spatial memory. **A** The escape latency to find platform of the Morris water maze in the acquisition trial. Three way ANOVA, F (3, 112) = 26.37, $p < 0.0001$, Tukey's multiple comparisons test: vehicle: static vs. AG1478: static: $p = 0.0038$, vehicle: static vs. vehicle: run: $p = 0.0002$, vehicle: static vs. vehicle: run: $p = 0.0020$, AG1478: static vs. vehicle: run, $p < 0.0001$, AG1478: static vs. AG1478: run: $p < 0.0001$. ***$p < 0.001$, ****$p < 0.0001$. $n = 8$. **B–D** No significantly difference among the four groups of total distance travelled, average velocity for total distance travelled, F (1, 28) = 0.8334, $p = 0.3691$, for average velocity, F (1, 28) = 0.8334, $p = 0.3691$, $p = 0.411$; for the percent time spent in the correct quadrant, $n = 8$. **D** The percent time spent in the correct quadrant in the probe trial. Two way ANOVA: F (1, 28) = 4.851, $p = 0.0360$, vehicle:static vs. AG1478:static: $p = 0.0436$, AG1478: static vs, vehicle: run: $p = 0.0062$, AG1478: static vs. AG1478: run: $p = 0.0027$. *$p < 0.05$, ***$p < 0.001$. $n = 8$. **E** Swimming trajectory images of the mice in the probe trial. **F** The number of times crossed the platform in the probe trial. Two way ANOVA: F (1, 28) = 2.597, $p = 0.1183$, Tukey's multiple comparisons test: vehicle:static vs. AG1478: static: $p = 0.0198$, vehicle: static vs. vehicle: run: $p = 0.0034$, vehicle: static vs. vehicle: run, $p = 0.0277$, AG1478: static vs.vehicle,: run: $p < 0.0001$, AG1478: static vs. AG1478: run: $p < 0.0001$. *$p < 0.05$, **$p < 0.01$, ****$p < 0.0001$. $n = 8$. **G**. Schematic experimental design of contextual and cued fear conditioning test. **H** Freezing levels of the contextual fear conditioning test. $n = 8$. Two way ANOVA: F (1, 28) = 3.189, $p = 0.0850$, Tukey's multiple comparisons test: vehicle: run: $p < 0.0001$, vehicle: static vs. vehicle: run: $p < 0.0001$, vehicle: static vs. AG1478: run: $p = 0.0008$, vehicle: static vs. AG1478: static vs. vehicle: run, $p < 0.0001$, AG1478: static vs. AG1478: run: $p < 0.0001$, vehicle: run vs. AG1478: run: $p < 0.0001$. ****$p < 0.0001$. $n = 8$. **I** Freezing levels of the cued fear conditioning test. Two way ANOVA: F (1, 28) = 2.127, $p = 0.1558$

compared to the control group as they spent more time in the center of the arena. However, no significant change was observed between the vehicle-treated static group and the AG1478-treated static group (Fig. 3A–D), indicating that treadmill running was effective in ameliorating anxiety, but may not be through the ErbB4 signaling pathway. These findings suggest that ErbB4 signaling plays a role in modulating hyperactivity, while treadmill running may be an effective means to reduce anxiety.

Effect of Treadmill Running on Working Memory and Partial Spatial Memory Compromised by AG1478

To analyze the impact of AG1478 treatment on working memory, we examined spontaneous alternations through the *T*-maze test. As shown in Figs. 3E and F, animals treated with AG1478 had fewer correct entries, indicating possible impairment of working memory caused by AG1478. However, after treadmill running, the decrease in correct entries was ameliorated, suggesting that ErbB4 signaling may play a significant role in enhancing working memory during running.

The Morris water maze (MWM) is a widely used technique for detecting spatial memory (Brandeis et al. 1989; McGarrity et al. 2017; Sakurai 1994). We used the MWM to evaluate cognitive functions related to adult hippocampal neurogenesis. In the acquisition trial, mice learned the location of a submerged platform in the target quadrant. Escape latency reduced over time, indicating that the mice in all test groups were able to learn the task. AG1478 resulted in a significant increase in escape latency for the platform during four days of training in the MWM when compared to the control group ($p < 0.005$), A significant decrease in escape latency was observed in the AG1478:run compared to both the AG1478:static and vehicle: static groups (Fig. 4A). In the probe trial, when the platform was removed, there were no significant differences in the total distance traveled and average velocity among the four groups (Fig. 4B–C). However, the percent time spent in the correct quadrant and numbers for crossing the platform were significantly lower in the AG1478: static group than the two vehicle:static groups (Fig. 4D–F). Notably, the AG1478 : run group showed a significant increase in this parameter after running, suggesting AG1478 may affect spatial learning.

To investigate the role of hippocampus-dependent memory, we measured non-spatial memory using a contextual and cued fear conditioning paradigm (Fig. 4G). The AG1478-treated mice exhibited decreased fear responses compared to the control group. However, after running, we observed a significant increase in freezing responses in the AG1478: run group (Fig. 4H), indicating that ErbB4 signaling enhances contextual fear memory. Later, we tested the mice for their auditory cue memory in a new shape context (context B) that is hippocampus independent; the results showed no significant difference between the AG1478-treated and control mice. Moreover, no abnormal nociceptive responses were observed between the static and running groups (Fig. 4I), suggesting that ErbB4 signaling can enhance hippocampus-dependent fear memory during running, whereas hippocampus-independent memory is unaffected.

Treadmill Running Effect on Pattern Separation Compromised by AG1478

In previous studies, it has been shown that contextual fear discrimination learning relies on the proper function of adult-generated DG cells (Kheirbek et al. 2012; McHugh et al. 2007) and is essential for the accuracy of memory encoding (Clelland et al. 2009). To discriminate between similar items in memory, distinct and high-fidelity representations must be formed via pattern separation. This process is thought to rely on the hippocampus, specifically the dentate gyrus, to orthogonalize overlapping inputs. Pattern separation is involved in context discrimination and the formation and retrieval processes of memory by storing the diversity of experience.

During the fear acquisition phase, pattern separation may be less necessary because the current context cannot be compared to a previous one. This could result in reduced activation in both structures which are important for retrieving contextual fear memories and recognition memory.

In this study, altered hippocampal neurogenesis was observed in two running groups of mice compared to two relative controls. To further investigate the signaling of hippocampal neurogenesis in running mice, a contextual fear discrimination paradigm was used to analyze their behavior. The mice were placed in a training chamber and received a foot shock for training. One hour later, the same mice were returned to the same context with a foot shock or to a modified context with no foot shock. They were allowed to explore each context for 3 min over five days, and their freezing behaviors were evaluated (Fig. 5A).

For the first 3 days, there was no difference in freezing behavior among the four groups (Figure S1A–D). On the fourth day, three groups could distinguish between contexts A and C, but the AG1478: static group showed only a trend towards lower freezing in context C relative to context A (Fig. 5B). On the fifth day, all mice exhibited similar levels between the two contexts, and the running groups showed significantly decreased freezing response in context C compared to context A (Fig. 5C).

The mice treated with AG1478 in the two groups displayed significantly decreased discrimination ratio compared to the running mice on the fourth day; however, on the fifth day, mice in all groups exhibited a significant increase in the discrimination ratio between the two similar contexts (Fig. 5D). Running significantly enhanced the discrimination ratio when compared to vehicle-treated mice.

The behavioral deficits induced by AG1478 were highly correlated with neurogenesis. These results suggest that treadmill running may compromise the effect of pattern separation on contextual fear discrimination learning when ErbB4 signaling is affected by AG1478. By reversing the AG1478-induced deficits through running, neurogenesis could be involved in this process.

Treadmill Running Effect on Intracellular Ca^{2+} Increases in PV^+ Neurons Attenuated by AG1478

In a previous study, running increases the number of PV^+ cells in the DG (Yi et al. 2020). To further assess the effect of AG1478 on PV activity, we injected AAV-EF1α-DIO-GCaMP6m-WPRE-hGH-pA into the DG of PV-Cre mice. We then observed intracellular calcium signals of cells in brain slice imaging. As shown in Fig. 6A–C, the intracellular Ca^{2+} levels in PV neurons of both groups were incomparable during the first 5 s. After that period, AG1478 treatment decreased the intracellular Ca^{2+} level in PV neurons compared to ACSF treatment. This difference became more significant over time.

Using in vivo calcium imaging, we further assessed the intracellular Ca^{2+} levels in the PV neurons during treadmill running. As shown in Fig. 6D–F, AG1478 treatment significantly decreased the intracellular Ca^{2+} levels in PV neurons compared to the control (vehicle: static), while running treatment (vehicle: run) showed significantly higher intracellular Ca^{2+} levels. The effect of running on the intracellular Ca^{2+} levels was attenuated by AG1478 treatment (AG1478: run), suggesting that ErbB4 signaling regulates the intracellular Ca^{2+} increase in PV neurons during animal movement.

Discussion

The family of ErbB receptors, including ErbB1-4, is fundamental to the proper physiological function of vertebrate tissue due to their involvement in numerous essential cellular functions such as cell growth, division, migration, adhesion, and apoptosis.. Among these receptors, ErbB1, and ErbB4 are expressed in dopamine and GABA neurons, while oligodendrocytes, astrocytes, and their precursors mainly present ERBB1, 2, and/or 3. Neural stem cells in the subventricular zone (SVZ) are highly enriched with ErbB1, whereas interneurons in the hippocampus and neocortex, as well as cerebellar Purkinje cells, express ErbB1 (Abe et al. 2009; Namba et al. 2009; Werner et al. 1988). Interestingly, ErbB1 activation in GABAergic neurons induces their de-differentiation, while ErbB2: ErbB4 heterodimers influence the morphological differentiation of hippocampal neurons (Gerecke et al. 2004; Nagano et al. 2007; Namba et al. 2006). ErbB3 expression is also observed in neural precursor cells in the adult hippocampus and contributes to their proliferation, although the expression is modest (Mahar et al. 2011). Furthermore, ErbB4 signals may accelerate neural differentiation in specific cell populations, potentially attenuating ErbB1 signaling (Woo et al. 2007). However, these processes also involve ErbB1, and therefore, the interplay between ErbB4 and ErbB1 needs to be further characterized to reveal the complete mechanism (Li et al. 2012) (Abe et al. 2009). Most importantly, PV^+ interneurons in the prefrontal cortex and hippocampus are $ErbB4^+$ (Bean et al., 2014). These findings suggest that the ErbB receptor family plays an essential role in numerous biological processes, including neural differentiation and migration. Thus, it is crucial to comprehend the distinct effects of these receptors to develop an understanding of the underlying pathophysiology of various neurological diseases.

AG1478, while commonly considered an inhibitor of ErbB4, has also been shown to effectively inhibit the activation of EGFR (ErbB1).The combinatorial assemblies of ErbB receptors, which have varying patterns of appearance,

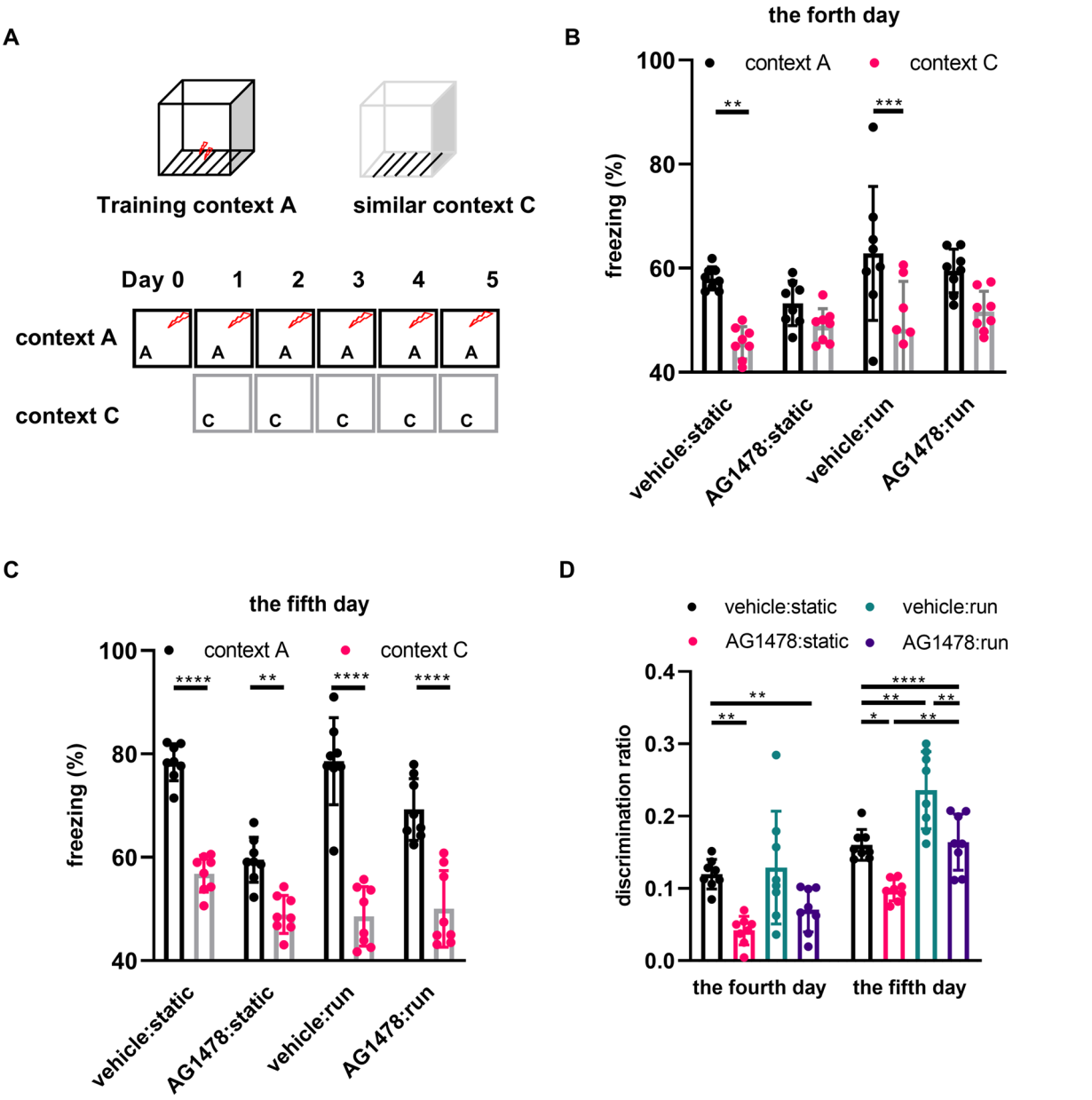

Fig. 5 AG1478 compromised movement-dependent effect on pattern separation. **A** Mice were tested in a contextual fear discrimination learning paradigm. Briefly, in two similar contexts, foot shook was only present in context A After several trials training in context A and C, mice could discriminate context A but not C as the cue of foot shook tested by freezing. **B** The fourth day of contextual fear discrimination learning. All mice without AG1478 treatment could discriminate between the context A and context **C** Two way ANOVA: F (3, 56) = 2.065, $p = 0.1152$. Tukey's multiple comparisons test: vehicle:static: $p = 0.0011$, vehicle: run: $p = 0.0001$. $^{*}p < 0.05$, $^{****}p < 0.0001$. $n = 8$. **C** The fifth day of contextual fear discrimination learning. All mice could discriminate between the context A and context C. Two way ANOVA: F (3, 56) = 8.104, $p = 0.0001$, Tukey's multiple comparisons test: vehicle: static: $p < 0.0001$, AG1478: static: $p = 0.0016$, vehicle: run: $p < 0.0001$, AG1478: run: $p < 0.0001$. $^{***}p < 0.001$, $^{****}p < 0.0001$. $n = 8$. **D** The discrimination ratio indicates that the learning ability of the mice changed along the learning period, AG1478 significantly decrease the discrimination ratio in the AG1478: static group compared to those in the vehicle: static group, which are enhanced by running in the fifth day. TWO way ANOVA: F (3, 56) = 2.439, $p = 0.074$, Tukey's multiple comparisons test: in the fourth day: vehicle: static vs. AG1478: static: $p = 0.0016$, AG1478: static vs. vehicle: run: $p = 0.0004$, vehicle: run vs. AG1478: run: $p = 0.03205$ in the fifth day: vehicle: static vs. AG1478: static: $p = 0.0172$, vehicle: static vs. vehicle: run: $p = 0.0023$, AG1478: static vs. vehicle: run: $p < 0.0001$, AG1478: static vs. AG1478: run: $p = 0.00908$, vehicle: run vs. AG1478: run: $p = 0.0042$. $^{*}p < 0.05$, $^{***}p < 0.001$, $^{****}p < 0.0001$. $n = 8$

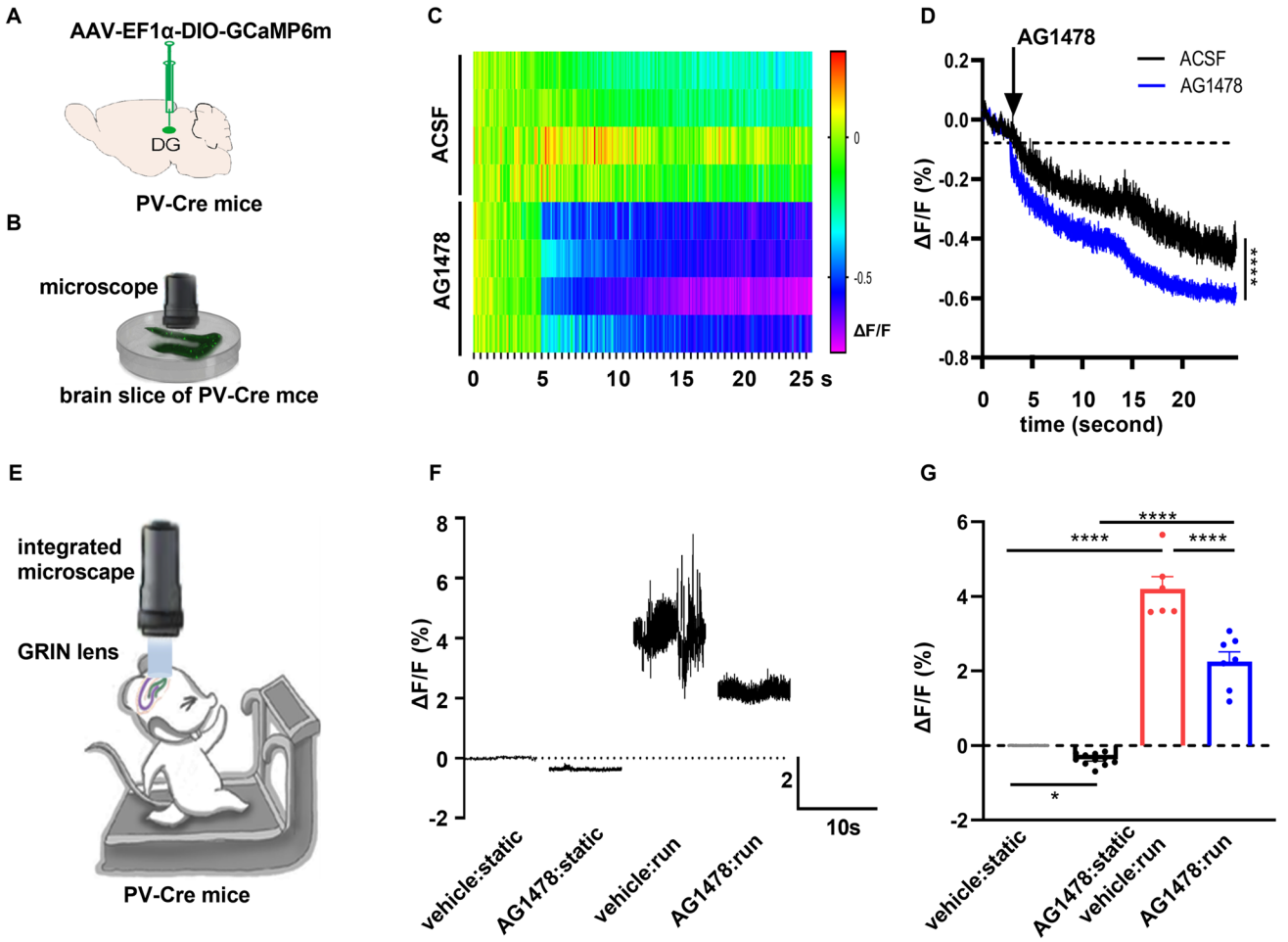

Fig. 6 Treadmill running effect on pattern separation compromised by AG1478. **A** Schematic diagram of virus injection into the DG of PV-Cre mice. **B** Schematic diagram of calcium imaging of brain slices in vitro. The fluorescence intensity of calcium ion signals in the DG region of brain slices was recorded by upright fluorescence microscopy under a patch-clamp perfusion system. **C** The representative calcium signal of PV neurons changed with time, the upper four cells changed the calcium ion signal under perfusion ACSF condition, and the lower four were under perfusion AG1478 condition. Each horizontal strip corresponds to the time course of the Ca^{2+} signal in each cell. **D** Traces of Ca^{2+} signals from PV neurons in brain slices from PV-Cre mice with injecting AAV-EF1α-DIO-GCaMP6m-WPRE-hGH-pA, $n = 11$ - 36 cells from 3 mice. Asterisks in black denote the significance between the ACSF-treated control and AG1478-treated brain slice. **E** Schematic of in vivo calcium imaging. Embed a GRIN lens onto the mouse head to DG and record real-time calcium signal fluorescence intensity by a head-mounted microscope. **F** Traces of Ca^{2+} signals from PV neurons in the DG of PV-Cre mice from the four groups. $n = 6$-11 cells from 4 mice. **G** Quantification of ΔF/F. Asterisks in black denote the significance between the control and AG1478-treated brain slice. Data are presented as means ± SEM. $^{*}p < 0.05$, $^{****}p < 0.0001$, 2-tailed Student's t test (**C**), Two way ANOVA with Bonferroni's post hoc test

seem to play a major role in determining their activity in different tissues (Kokai et al. 1989). Local receptor-ligand interactions have also been found to be crucial in determining their activities (Olayioye et al. 2000), (Holbro and Hynes 2004; Qian et al. 1994). Differential expression and localization patterns of ErbB receptors and their ligands in various tissues also affect their coordinated functions (Gerecke et al. 2001; Shelly et al. 2003). The importance of interactions between NRG1 expressed by ganglion neurons and ErbB2/ErbB4 expressed by Corti supporting cells for the survival of adult spiral ganglion neurons (Stankovic et al. 2004). Another study showed that activation of ErbB1/ErbB2 signaling by TGF in tanycytes, a type of ependymoglial cell, induces cellular plasticity and the release of TGF1 (Prevot et al. 2003). Similarly, NRG1 signaling through ErbB2/ErbB4 has been found to aid neurite extension and arborization in cultured hippocampal neurons (Gerecke et al. 2004) When conducting experiments to detect ErbB receptor activation, researchers typically measure the quantity of tyrosine phosphorylation as an indicator of activation magnitude or occurrence. With the exception of ErbB2, all ErbB receptors have known ligands, while all but ErbB3 have relatively active kinase domains. EebB2 has minimal activity in ligand binding, but it is a favored partner for heterodimerization

with other ErbB receptors. Although ErbB3 has minimal kinase activity, it is much reduced compared to other ErbB receptors. EGF-family ligands bind and activate EGFR, whereas heregulin-family ligands, also called neuregulins (NRG), interact with ErbB3 and ErbB4. No ligand has been identified for ErbB2, which instead acts as a preferred dimerization partner for other ErbB receptors in both ligand-dependent and -independent manners (Kumagai et al. 2001, 2003; Riese and Stern 1998).

Growing evidence has demonstrated that the NRG1-ErbB4 pathway affects neurogenesis in both the embryonic and adult rostral migratory stream (RMS) of mice (Curtis et al. 2007). ErbB4 expression is detected in projection fields of the prefrontal cortex and ventral hippocampus, including the ventral striatum. As such, Nrg1/ErbB4 signaling might be required to maintain normal hippocampal structures and may influence related behaviors. The ErbB4 receptor, specifically its JM-a-derived 4ICD fragment, has been shown to promote neuronal progenitor migration (Flames et al. 2004). In particular, the number of mature newborn neurons ($BrdU^+NeuN^+$) decreased in the hippocampus of mice after deleting ErbB4 in PV neurons (Zhang et al. 2018). Phosphorylation of the ErbB4 receptor leads to the recruitment of adaptor/effecter molecules (Olayioye et al. 2000) and activates numerous downstream signaling pathways crucial to neuronal development, migration, axonal navigation, and synaptic function (Mei and Nave 2014). These findings may be beneficial for understanding ErbB4 and NRGs as modulators of the proliferation and migration of neural stem and progenitor cells. The present study investigated the effects of ErbB4 inhibition using AG1478, an ErbB signaling inhibitor, on neurogenesis and cognitive function in mice. The results showed a significant decrease in the relative total ErbB4 levels in the hippocampus of the AG1478-treated mice compared to the vehicle control group. The decreased relative pErbB4 levels in the hippocampus of AG1478: static mice could be attenuated by running (Fig. 1C, D). Phosphorylation of ErbB4 activates downstream signaling pathways crucial to neuronal development, migration, axonal navigation, and synaptic function (Mei and Nave 2014), which may explain the observed deficits in neurogenesis and cognitive function. These included phosphorylation events mediated through STAT3 activation-a typical pathogenic pathway (Liu et al. 2012, 2013), ERK MAP kinase, and Akt pathway activation (Wandinger et al. 2016), which account for a variety of phosphorylation-dependent signaling mechanisms known to contribute to cell survival and proliferation.

Neurogenesis is a multistep process whereby precursor cells undergo lineage-directed cell division to produce immature neurons, of which only a fraction are selected to survive and contribute to hippocampal function. Activation of ErbB receptors impacts cell proliferation, migration, differentiation, and apoptosis in various cell types (Liu et al. 2018). BrdU labeling data showed that ablation of ErbB4 in PV neurons promotes hippocampal neural progenitor cell (NPC) proliferation (Zhang et al. 2018). In contrast, our study found that AG1478 treatment blocked the running-induced activation of ErbB4 and led to decreased proliferation of hippocampal NPCs with deficits in neuronal survival. This suggests that the mechanism of running may be related to the activation of ErbB4 signaling, which is crucial for cell proliferation and survival. Ki67 is expressed in the cell cycle during all except the G0 and early G1 phases and is used to provide evidence of proliferation (Gerdes et al. 1983). To pharmacologically dissect ErbB4 functions on neurogenesis, we treated mice with AG1478, an inhibitor of ErbB signaling, to inhibit ErbB4. Our report of putatively dividing and synthetic cells indicates proliferation and survival cells in the DG of the running mice, as previously suggested. However, AG1478 blocked running-induced activations of ErbB4, and it exhibited decreased proliferation of hippocampal neural progenitor cells with deficits in neuronal survival. These further suggest that the mechanism of running may be related to the activation of ErbB4 signaling. Future studies might be needed to make firmer conclusions about the exact time course of running effects on various neurons by employing thymidine analogs.

To understand the contributions of cognitive function, we sought to determine which aspects of cognition could be rescued. Behavioral analysis revealed AG1478-treated mice showed hyperactivity without changes in anxiety-related behavior in the OFT task. In the T-maze and the MWM task, we found significant changes in working memory and spatial learning by running. Additionally, AG1478 treatment decreased contextual fear memory without alterations in cued fear conditioning, while treadmill running rescued the contextual fear memory. These findings suggest that treadmill running may be involved in hippocampus-dependent cognitive functions.

The adult brain produces new neurons in the hippocampus, a region important for learning and memory. Recent studies reveal that a decrease in new neurons can impair pattern separation, a process critical for discriminating similar experiences (Anacker and Hen 2017; Lepousez et al. 2015). On the other hand, an increase in new neurons promotes pattern separation and executive function. To examine this phenomenon, we rendered the contextual fear discrimination learning paradigms to test pattern separation. Our study found that the mice treated with AG1478 had a decreased ability to discriminate between two similar contexts, revealing a disruption in pattern separation. However, when the mice underwent physical exercise, their performance on the pattern separation task improved. We also observed a decrease in new neurons in the treated mice, as indicated by the ki67-positive and $BrdU^+NeuN^+$ labels.

The changes in behavior and neurogenesis are likely to increase the responsiveness of granule cells in the hippocampus to stimulation during cognitive tasks involving context and spatial memory (Deng et al. 2009; Saxe et al. 2006). Disturbances in the maturation of the hippocampus have been reported in psychiatric disorders such as schizophrenia and depression (Hagihara et al. 2013), indicating the importance of understanding the cellular processes underlying these conditions. Our study sheds light on a potential therapeutic target for improving cognitive function in psychiatric disorders. Further investigations are necessary to explore the involvement of signaling pathways mediated by the ErbB4 receptor in these disorders.

In neuroscience, neurons play a key role in maintaining normal brain function. The firing of an action potential and the transmission of synaptic input contribute to rapid changes in intracellular free [Ca^{2+}] levels in neurons (Dur-e-Ahmad et al. 2011; Miyakawa et al. 1992). Among the various types of neurons that make up the brain, PV^+ interneurons are a critical subpopulation, despite comprising less than 2% of all neurons in the hippocampus (Kontou et al. 2021). These neurons express parvalbumin (PV), a Ca^{2+}-binding protein vital for proper neuronal function. As a member of the family of EF-hand Ca^{2+}-binding proteins (CaBPs), PV serves as a component of the Ca^{2+}-signaling toolkit, acting as a Ca2 + buffer (Berridge et al. 2003). Knockout mice lacking PV ($PV^{-/-}$) exhibit altered kinetics of intracellular Ca^{2+} signals, modulating the short-term synaptic plasticity of hippocampal PV neuron synapses (Vreugdenhil et al. 2003). Understanding the physiological roles of PV^+ interneurons is therefore crucial for comprehending the intricate workings of the brain. The present study also investigated the involvement of intracellular Ca^{2+} activity in PV^+ interneurons in the effects of AG1478 and treadmill running. PV^+ interneurons play crucial roles in shaping neuronal network activity (Kontou et al. 2021), and our results showed that calcium activity levels increased in the population of PV cells of the DG after treadmill running, whereas AG1478 treatment led to a distinct decrease in this calcium activity.

In summary, our findings provide strong evidence that AG1478 is capable of inducing neurogenesis deficits in the adult hippocampus and impairing hippocampus-dependent memory. Additionally, the ErbB4 signaling pathway is implicated in altering hippocampal interneuron activity and animal behavior. These results underscore the interactions between intracellular Ca^{2+} activity in PV cells and neurogenesis, shedding light on potential targets for preventing and treating of neuropsychiatric disorders such as schizophrenia and depression. Further studies are needed to better understand the specific mechanisms involved.

Supplementary Information The online version contains supplementary material available at https://doi.org/10.1007/s10571-023-01439-0.

Author Contributions YL: conceived the study and participated in the experiment design. YY and YS: performed the experiments, carried out the functional analysis, and drafted the manuscript. YS: contributed to the experiment design and manuscript preparation. All authors read and approved the final manuscript.

Funding This work was supported by grants from the National Natural Science Foundation of China (82071508), the Natural Science Foundation of Hubei Province (2020CFB727), and the Medical Research Project of Wuhan City (WZ20C19).

Data Availability Not applicable.

Declarations

Conflict of interest The authors declare that the research was conducted in without any commercial or financial relationships that could be construed as a potential conflict of interest.

Ethical Approval The animal study was reviewed and approved by the Animal Welfare Committee of Huazhong University of Science and Technology. Protocols for animal experiments were approved by the Animal Experimental Ethics Committee of the Huazhong University of Science and Technology (Approval code: 82071508) on September 27, 2020.

Consent for Publication Not applicable.

References

Abe Y, Namba H, Zheng Y, Nawa H (2009) In situ hybridization reveals developmental regulation of ErbB1-4 mRNA expression in mouse midbrain: implication of ErbB receptors for dopaminergic neurons. Neuroscience 161:95–110

Albarran-Zeckler RG, Brantley AF, Smith RG (2012) Growth hormone secretagogue receptor (GHS-R1a) knockout mice exhibit improved spatial memory and deficits in contextual memory. Behav Brain Res 232:13–19

Anacker C, Hen R (2017) Adult hippocampal neurogenesis and cognitive flexibility - linking memory and mood. Nat Rev Neurosci 18:335–346

Bean JC, Lin TW, Sathyamurthy A, Liu F, Yin DM, Xiong WC, Mei L (2014) Genetic labeling reveals novel cellular targets of schizophrenia susceptibility gene: distribution of GABA and non-GABA ErbB4-positive cells in adult mouse brain. J Neurosci 34:13549–13566

Berridge MJ, Bootman MD, Roderick HL (2003) Calcium signalling: dynamics, homeostasis and remodelling. Nat Rev Mol Cell Biol 4:517–529

Brandeis R, Brandys Y, Yehuda S (1989) The use of the Morris Water Maze in the study of memory and learning. Int J Neurosci 48:29–69

Cai MX, Shi XC, Chen T, Tan ZN, Lin QQ, Du SJ, Tian ZJ (2016) Exercise training activates neuregulin 1/ErbB signaling and promotes cardiac repair in a rat myocardial infarction model. Life Sci 149:1–9

Cetin A, Komai S, Eliava M, Seeburg PH, Osten P (2006) Stereotaxic gene delivery in the rodent brain. Nat Protoc 1:3166–3173

Christian KM, Song H, Ming GL (2014) Functions and dysfunctions of adult hippocampal neurogenesis. Annu Rev Neurosci 37:243–262

Clelland CD, Choi M, Romberg C, Clemenson GD Jr, Fragniere A, Tyers P, Jessberger S, Saksida LM, Barker RA, Gage FH et al (2009) A functional role for adult hippocampal neurogenesis in spatial pattern separation. Science 325:210–213

Curtis MA, Kam M, Nannmark U, Anderson MF, Axell MZ, Wikkelso C, Holtas S, van Roon-Mom WM, Bjork-Eriksson T, Nordborg C et al (2007) Human neuroblasts migrate to the olfactory bulb via a lateral ventricular extension. Science 315:1243–1249

Deng W, Saxe MD, Gallina IS, Gage FH (2009) Adult-born hippocampal dentate granule cells undergoing maturation modulate learning and memory in the brain. J Neurosci 29:13532–13542

Deng C, Pan B, Engel M, Huang XF (2013) Neuregulin-1 signalling and antipsychotic treatment: potential therapeutic targets in a schizophrenia candidate signalling pathway. Psychopharmacology 226:201–215

Dur-e-Ahmad M, Imran M, Gul A (2011) Calcium dynamics in dendritic spines: a link to structural plasticity. Math Biosci 230:55–66

Faghihi F, Moustafa AA (2015) A computational model of pattern separation efficiency in the dentate gyrus with implications in schizophrenia. Front Syst Neurosci 9:42

Flames N, Long JE, Garratt AN, Fischer TM, Gassmann M, Birchmeier C, Lai C, Rubenstein JL, Marin O (2004) Short- and long-range attraction of cortical GABAergic interneurons by neuregulin-1. Neuron 44:251–261

Gerdes J, Schwab U, Lemke H, Stein H (1983) Production of a mouse monoclonal antibody reactive with a human nuclear antigen associated with cell proliferation. Int J Cancer 31:13–20

Gerecke KM, Wyss JM, Karavanova I, Buonanno A, Carroll SL (2001) ErbB transmembrane tyrosine kinase receptors are differentially expressed throughout the adult rat central nervous system. J Comp Neurol 433:86–100

Gerecke KM, Wyss JM, Carroll SL (2004) Neuregulin-1beta induces neurite extension and arborization in cultured hippocampal neurons. Mol Cell Neurosci 27:379–393

Hagihara H, Takao K, Walton NM, Matsumoto M, Miyakawa T (2013) Immature dentate gyrus: an endophenotype of neuropsychiatric disorders. Neural Plast 2013:318596

Holbro T, Hynes NE (2004) ErbB receptors: directing key signaling networks throughout life. Annu Rev Pharmacol Toxicol 44:195–217

Hughes RN (2004) The value of spontaneous alternation behavior (SAB) as a test of retention in pharmacological investigations of memory. Neurosci Biobehav Rev 28:497–505

Kempermann G, Kuhn HG, Gage FH (1997) More hippocampal neurons in adult mice living in an enriched environment. Nature 386:493–495

Kheirbek MA, Tannenholz L, Hen R (2012) NR2B-dependent plasticity of adult-born granule cells is necessary for context discrimination. J Neurosci 32:8696–8702

Kokai Y, Myers JN, Wada T, Brown VI, LeVea CM, Davis JG, Dobashi K, Greene MI (1989) Synergistic interaction of p185c-neu and the EGF receptor leads to transformation of rodent fibroblasts. Cell 58:287–292

Kontou G, Antonoudiou P, Podpolny M, Szulc BR, Arancibia-Carcamo IL, Higgs NF, Lopez-Domenech G, Salinas PC, Mann EO, Kittler JT (2021) Miro1-dependent mitochondrial dynamics in parvalbumin interneurons. Elife 10:e65215

Kumagai T, Davis JG, Horie T, O'Rourke DM, Greene MI (2001) The role of distinct p185neu extracellular subdomains for dimerization with the epidermal growth factor (EGF) receptor and EGF-mediated signaling. Proc Natl Acad Sci USA 98:5526–5531

Kumagai T, Katsumata M, Hasegawa A, Furuuchi K, Funakoshi T, Kawase I, Greene MI (2003) Role of extracellular subdomains of p185c-neu and the epidermal growth factor receptor in ligand-independent association and transactivation. Proc Natl Acad Sci USA 100:9220–9225

Lalonde R, Lewis TL, Strazielle C, Kim H, Fukuchi K (2003) Transgenic mice expressing the betaAPP695SWE mutation: effects on exploratory activity, anxiety, and motor coordination. Brain Res 977:38–45

Leem YH, Kato M, Chang H (2018) Regular exercise and creatine supplementation prevent chronic mild stress-induced decrease in hippocampal neurogenesis via Wnt/GSK3beta/beta-catenin pathway. J Exerc Nutrition Biochem 22:1–6

Lepousez G, Nissant A, Lledo PM (2015) Adult neurogenesis and the future of the rejuvenating brain circuits. Neuron 86:387–401

Li H, Chou SJ, Hamasaki T, Perez-Garcia CG, O'Leary DD (2012) Neuregulin repellent signaling via ErbB4 restricts GABAergic interneurons to migratory paths from ganglionic eminence to cortical destinations. Neural Dev 7:10

Liu M, Amodu AS, Pitts S, Patrickson J, Hibbert JM, Battle M, Ofori-Acquah SF, Stiles JK (2012) Heme mediated STAT3 activation in severe malaria. PLoS ONE 7:e34280

Liu M, Wilson NO, Hibbert JM, Stiles JK (2013) STAT3 regulates MMP3 in heme-induced endothelial cell apoptosis. PLoS ONE 8:e71366

Liu M, Solomon W, Cespedes JC, Wilson NO, Ford B, Stiles JK (2018) Neuregulin-1 attenuates experimental cerebral malaria (ECM) pathogenesis by regulating ErbB4/AKT/STAT3 signaling. J Neuroinflammation 15:104

Mahar I, Tan S, Davoli MA, Dominguez-Lopez S, Qiang C, Rachalski A, Turecki G, Mechawar N (2011) Subchronic peripheral neuregulin-1 increases ventral hippocampal neurogenesis and induces antidepressant-like effects. PLoS ONE 6:e26610

Mao Y, Ge X, Frank CL, Madison JM, Koehler AN, Doud MK, Tassa C, Berry EM, Soda T, Singh KK et al (2009) Disrupted in schizophrenia 1 regulates neuronal progenitor proliferation via modulation of GSK3beta/beta-catenin signaling. Cell 136:1017–1031

McGarrity S, Mason R, Fone KC, Pezze M, Bast T (2017) Hippocampal neural disinhibition causes attentional and memory deficits. Cereb Cortex 27:4447–4462

McHugh TJ, Jones MW, Quinn JJ, Balthasar N, Coppari R, Elmquist JK, Lowell BB, Fanselow MS, Wilson MA, Tonegawa S (2007) Dentate gyrus NMDA receptors mediate rapid pattern separation in the hippocampal network. Science 317:94–99

McNaughton BL, Barnes CA, Rao G, Baldwin J, Rasmussen M (1986) Long-term enhancement of hippocampal synaptic transmission and the acquisition of spatial information. J Neurosci 6:563–571

Mei L, Nave KA (2014) Neuregulin-ERBB signaling in the nervous system and neuropsychiatric diseases. Neuron 83:27–49

Mei L, Xiong WC (2008) Neuregulin 1 in neural development, synaptic plasticity and schizophrenia. Nat Rev Neurosci 9:437–452

Mertens J, Wang QW, Kim Y, Yu DX, Pham S, Yang B, Zheng Y, Diffenderfer KE, Zhang J, Soltani S et al (2015) Differential responses to lithium in hyperexcitable neurons from patients with bipolar disorder. Nature 527:95–99

Miyakawa H, Ross WN, Jaffe D, Callaway JC, Lasser-Ross N, Lisman JE, Johnston D (1992) Synaptically activated increases in Ca2+ concentration in hippocampal CA1 pyramidal cells are primarily due to voltage-gated Ca2+ channels. Neuron 9:1163–1173

Montag-Sallaz M, Montag D (2003) Severe cognitive and motor coordination deficits in tenascin-R-deficient mice. Genes Brain Behav 2:20–31

Nagano T, Namba H, Abe Y, Aoki H, Takei N, Nawa H (2007) In vivo administration of epidermal growth factor and its homologue attenuates developmental maturation of functional excitatory synapses in cortical GABAergic neurons. Eur J Neurosci 25:380–390

Namba H, Nagano T, Iwakura Y, Xiong H, Jourdi H, Takei N, Nawa H (2006) Transforming growth factor alpha attenuates the functional

expression of AMPA receptors in cortical GABAergic neurons. Mol Cell Neurosci 31:628–641
Namba H, Zheng Y, Abe Y, Nawa H (2009) Epidermal growth factor administered in the periphery influences excitatory synaptic inputs onto midbrain dopaminergic neurons in postnatal mice. Neuroscience 158:1731–1741
Olayioye MA, Neve RM, Lane HA, Hynes NE (2000) The ErbB signaling network: receptor heterodimerization in development and cancer. EMBO J 19:3159–3167
Pajonk FG, Wobrock T, Gruber O, Scherk H, Berner D, Kaizl I, Kierer A, Muller S, Oest M, Meyer T et al (2010) Hippocampal plasticity in response to exercise in schizophrenia. Arch Gen Psychiatry 67:133–143
Prevot V, Rio C, Cho GJ, Lomniczi A, Heger S, Neville CM, Rosenthal NA, Ojeda SR, Corfas G (2003) Normal female sexual development requires neuregulin-erbB receptor signaling in hypothalamic astrocytes. J Neurosci: off J Soc Neurosci 23:230–239
Qian X, Dougall WC, Hellman ME, Greene MI (1994) Kinase-deficient neu proteins suppress epidermal growth factor receptor function and abolish cell transformation. Oncogene 9:1507–1514
Riese DJ 2nd, Stern DF (1998) Specificity within the EGF family/ErbB receptor family signaling network. BioEssays 20:41–48
Sahay A, Scobie KN, Hill AS, O'Carroll CM, Kheirbek MA, Burghardt NS, Fenton AA, Dranovsky A, Hen R (2011) Increasing adult hippocampal neurogenesis is sufficient to improve pattern separation. Nature 472:466–470
Sakurai Y (1994) Involvement of auditory cortical and hippocampal neurons in auditory working memory and reference memory in the rat. J Neurosci 14:2606–2623
Saxe MD, Battaglia F, Wang JW, Malleret G, David DJ, Monckton JE, Garcia AD, Sofroniew MV, Kandel ER, Santarelli L et al (2006) Ablation of hippocampal neurogenesis impairs contextual fear conditioning and synaptic plasticity in the dentate gyrus. Proc Natl Acad Sci U S A 103:17501–17506
Shelly M, Mosesson Y, Citri A, Lavi S, Zwang Y, Melamed-Book N, Aroeti B, Yarden Y (2003) Polar expression of ErbB-2/HER2 in epithelia. Bimodal regulation by Lin-7. Dev Cell 5:475–486
Shoji H, Takao K, Hattori S, Miyakawa T (2014) Contextual and cued fear conditioning test using a video analyzing system in mice. J vis Exp. https://doi.org/10.3791/50871-v
So JH, Huang C, Ge M, Cai G, Zhang L, Lu Y, Mu Y (2017) Intense exercise promotes adult hippocampal neurogenesis but not spatial discrimination. Front Cell Neurosci 11:13
Stankovic K, Rio C, Xia A, Sugawara M, Adams JC, Liberman MC, Corfas G (2004) Survival of adult spiral ganglion neurons requires erbB receptor signaling in the inner ear. J Neurosci: off J Soc Neurosci 24:8651–8661
van Praag H, Kempermann G, Gage FH (1999) Running increases cell proliferation and neurogenesis in the adult mouse dentate gyrus. Nat Neurosci 2:266–270
Vreugdenhil M, Jefferys JG, Celio MR, Schwaller B (2003) Parvalbumin-deficiency facilitates repetitive IPSCs and gamma oscillations in the hippocampus. J Neurophysiol 89:1414–1422
Wandinger SK, Lahortiga I, Jacobs K, Klammer M, Jordan N, Elschenbroich S, Parade M, Jacoby E, Linders JT, Brehmer D et al (2016) Quantitative phosphoproteomics analysis of ERBB3/ERBB4 signaling. PLoS ONE 11:e0146100
Weglicki WB, Kramer JH, Spurney CF, Chmielinska JJ, Mak IT (2012) The EGFR tyrosine kinase inhibitor tyrphostin AG-1478 causes hypomagnesemia and cardiac dysfunction. Can J Physiol Pharmacol 90:1145–1149
Wen L, Lu YS, Zhu XH, Li XM, Woo RS, Chen YJ, Yin DM, Lai C, Terry AV Jr, Vazdarjanova A et al (2010) Neuregulin 1 regulates pyramidal neuron activity via ErbB4 in parvalbumin-positive interneurons. Proc Natl Acad Sci USA 107:1211–1216
Werner MH, Nanney LB, Stoscheck CM, King LE (1988) Localization of immunoreactive epidermal growth factor receptors in human nervous system. J Histochem Cytochem 36:81–86
Woo RS, Li XM, Tao Y, Carpenter-Hyland E, Huang YZ, Weber J, Neiswender H, Dong XP, Wu J, Gassmann M et al (2007) Neuregulin-1 enhances depolarization-induced GABA release. Neuron 54:599–610
Yi Y, Song Y, Lu Y (2020) Parvalbumin interneuron activation-dependent adult hippocampal neurogenesis is required for treadmill running to reverse schizophrenia-like phenotypes. Front Cell Dev Biol 8:24
Zhang H, He X, Mei Y, Ling Q (2018) Ablation of ErbB4 in parvalbumin-positive interneurons inhibits adult hippocampal neurogenesis through down-regulating BDNF/TrkB expression. J Comp Neurol 526:2482–2492